CORE THERMAL HYDRAULIC BEHAVIOR DURING THE REFLOOD PHASE OF COLD-LEG LBLOCA EXPERIMENTS USING THE ATLAS TEST FACILITY

SEOK CHO*, HYUN-SIK PARK, KI-YONG CHOI, KYOUNG-HO KANG, WON-PIL BAEK and YEON-SIK KIM
Thermal Hydraulics Safety Research Division, Korea Atomic Energy Research Institute
1045 Daedeokdaero, Yuseong, Daejeon, 305-353, Korea
*Corresponding author. E-mail : scho@kaeri.re.kr

Received February 4, 2009
Accepted for Publication August 26, 2009

Several experimental tests to simulate a reflood phase of a cold-leg LBLOCA of the APR1400 have been performed using the ATLAS facility. This paper describes the related experimental results with respect to the thermal-hydraulic behavior in the core and the system-core interactions during the reflood phase of the cold-leg LBLOCA conditions. The present descriptions will be focused on the LB-CL-09, LB-CL-11, LB-CL-14, and LB-CL-15 tests performed using the ATLAS. The LB-CL-09 is an integral effect test with conservative boundary condition; the LB-CL-11 and -14 are integral effect tests with realistic boundary conditions, and the LB-CL-15 is a separated effect test. The objectives of these tests are to investigate the thermal-hydraulic behavior during an entire reflood phase and to provide reliable experimental data for validating the LBLOCA analysis methodology for the APR1400. The initial and boundary conditions were obtained by applying scaling ratios to the MARS simulation results for the LBLOCA scenario of the APR1400. The ECC water flow rate from the safety injection tanks and the decay heat were simulated from the start of the reflood phase. The simulated core power was controlled to be 1.2 times that of the ANS-73 decay heat curve for LB-CL-09 and 1.02 times that of the ANS-79 decay curve for LB-CL-11, -14, and -15. The simulated ECC water flow rate from the high pressure safety injection pump was 0.32 kg/s. The present experimental data showed that the cladding temperature behavior is closely related to the collapsed water level in the core and the downcomer.

KEYWORDS : LBLOCA, APR1400, ATLAS, Reflood, System-Core Interaction

1. INTRODUCTION

The large number of reflooding experiments for separated effect observation with tubes and bundles performed in the seventies and eighties established an understanding of the reflooding heat transfer and two-phase flow phenomena [1]. These experiments [2-4] were very useful for model development, validation of the thermal-hydraulic modeling of reflooding, and code assessment. KAERI (Korea Atomic Energy Research Institute) began the operation of the ATLAS (Advanced Thermal-Hydraulic Test Loop for Accident Simulation) in 2007 [5]. The ATLAS is a thermal-hydraulic integral effect test facility for evolutionary pressurized water reactors such as the APR1400 and OPR1000.

In a nuclear reactor system, the emergency core cooling system (ECCS) provides an independent backup to the reactor coolant system, ensuring that a failure of the reactor piping will not result in an unacceptably high peak clad temperature, fuel failure, and release of fission products to the containment atmosphere. In the APR1400, four mechanically separated emergency core cooling (ECC) trains, each of which consists of a high pressure safety injection pump (SIP) and a safety injection tank (SIT), are connected to a direct vessel injection (DVI) nozzle located about 2.1 m above the centerline of a cold leg. Since the emergency core cooling (ECC) water is injected directly into the upper part of the reactor vessel downcomer, the thermal-hydraulic phenomena during the cold leg LBLOCA condition could be quite different from those observed in the existing commercial PWRs with the cold leg injection (CLI) mode of ECCS due to an increased ECC bypass rate [5].

Another important safety issue of the APR1400, which must be addressed to obtain license from the Korean regulation organization, is the thermal hydraulics occurring in the downcomer region during the late reflood phase for a large break LOCA (LBLOCA). In particular, a downcomer boiling will degrade the core cooling capability in two different ways: reducing the subcooling of the coolant

entering the core and reducing the hydraulic head due to boiling along the downcomer.

The objectives of these tests are to investigate the thermal-hydraulic characteristics in the core region during the reflood phase of the cold-leg LBLOCA, and to provide reliable experimental data for validating the LBLOCA analysis methodology for the APR1400. The ATLAS can be used to provide comprehensive experimental data on an ECC bypass and core cooling under the conditions in which the downcomer region interacts with the reactor core region. This paper presents the related experimental results for the ATLAS during the reflood phase of the LBLOCA tests named LB-CL-09, -11, -14 and -15, and provides related technical descriptions from the view point of the system-core interactions on the thermal-hydraulic behavior in the core of the ATLAS facility. The LB-CL-09, -11, and -14 are integral effect tests for the reflood phase of a LBLOCA to investigate the thermal-hydraulic characteristics. The LB-CL-09 is a typical test for a conservative condition, and the LB-CL-11 is for a best-estimate condition. The LB-CL-14 is also for a best-estimate condition and, furthermore, it includes the effects of a radial power distribution. The LB-CL-15 is a separate effect test to validate the reflood models of the best-estimate system analysis code such as the multidimensional analysis of reactor safety (MARS) for quench phenomena under low flow rate ECC injection conditions.

2. A BRIEF DESCRIPTION OF THE ATLAS

The ATLAS (Advanced Thermal-Hydraulic Test Loop for Accident Simulation) has the same two-loop features as the APR1400, the reference PWR plant of the ATLAS facility, and is designed according to the well-known scaling method suggested by Ishii and Kataoka [6] to simulate the various test scenarios as realistically as possible. The ATLAS was designed to have a 1/2 height, a 1/288 volume scale ratio, a full-pressure simulation of the reference plant, a geometrical similarity with the APR1400, including two hot legs and four cold legs, direct vessel injection (DVI), an integrated annular downcomer, etc. According to the scaling law, the reduced height scaling has time-reducing results in the model. For the one-half-height facility, the ratio of the time scale of the test facility (scaled-down model) to that of the prototype is $1/\sqrt{2}$, i.e., the phenomena in the test facility progress faster than those in the prototypic design. The friction factors in the scaled model are maintained the same as those of the prototype. The hydraulic diameter of the scaled model is maintained the same as that of the prototype to preserve the prototypical conditions for the heat transfer coefficient. Major scaling parameters of the ATLAS are summarized in Table 1. Detailed technical descriptions of the ATLAS can be found in Ref. [7].

The fluid system of the ATLAS consists of a primary system, a secondary system, a safety injection system, a break simulating system, a containment simulating system, and auxiliary systems as schematically depicted in Fig. 1. The primary system includes a reactor vessel, two hot legs, four cold legs, a pressurizer, four reactor coolant pumps, and two steam generators. The secondary system of the ATLAS is simplified to be of a circulating loop-type. The steam generated at two steam generators is condensed in a direct condenser tank and the condensed feedwater is again injected into the steam generators. Most of the safety injection features of the APR1400 and the OPR1000 are incorporated into the safety injection system of the ATLAS. It consists of four safety injection tanks (SITs), and safety injection pumps (SIPs).

The core simulator is designed to preserve the distributions of the temperature, pressure, coolant volume, flow, and flow area. The core simulator is also designed to preserve the hydraulic diameter for a realistic simulation of the local phenomena. The ATLAS core simulator consists of 390 electrically heated heater rods, six unheated rods, and five core guide tubes with ten spacer grids. It is shielded by a core shroud and a core support barrel. The core simulator can be heated indirectly by a 3-phase, 440 V AC power supply and be divided into three control segment groups (G1, G2 and G3) for a radial power distribution, as presented in Fig. 2. The axial power distribution along the heated length of the heater rod has a chopped cosine shape and is depicted in Fig. 3 with the axial locations of the seven spacer grids installed in the heated section. The maximum core power was limited to 10 % (i.e., about 2.0 MWe) of the scaled nominal power of the reference plant due to power limitations at KAERI.

The control and data acquisition system of the ATLAS

Table 1. Major Scaling Parameters of the ATLAS

Parameters	Scaling law	ATLAS design
Length	l_{oR}	1/2
Diameter	d_{oR}	1/12
Area	d^2_{oR}	1/144
Volume	$l_{oR}d^2_{oR}$	1/288
Core ΔT	ΔT_{oR}	1
Velocity	$l^{1/2}_{oR}$	$1/\sqrt{2}$
Time	$l^{1/2}_{oR}$	$1/\sqrt{2}$
Power/Volume	$l^{-1/2}_{oR}$	$\sqrt{2}$
Heat flux	$l^{-1/2}_{oR}$	$\sqrt{2}$
Core power	$l^{1/2}_{oR}d^2_{oR}$	1/203.6
Flow rate	$l^{1/2}_{oR}d^2_{oR}$	1/203.6
Pressure drop	l_{oR}	1/2

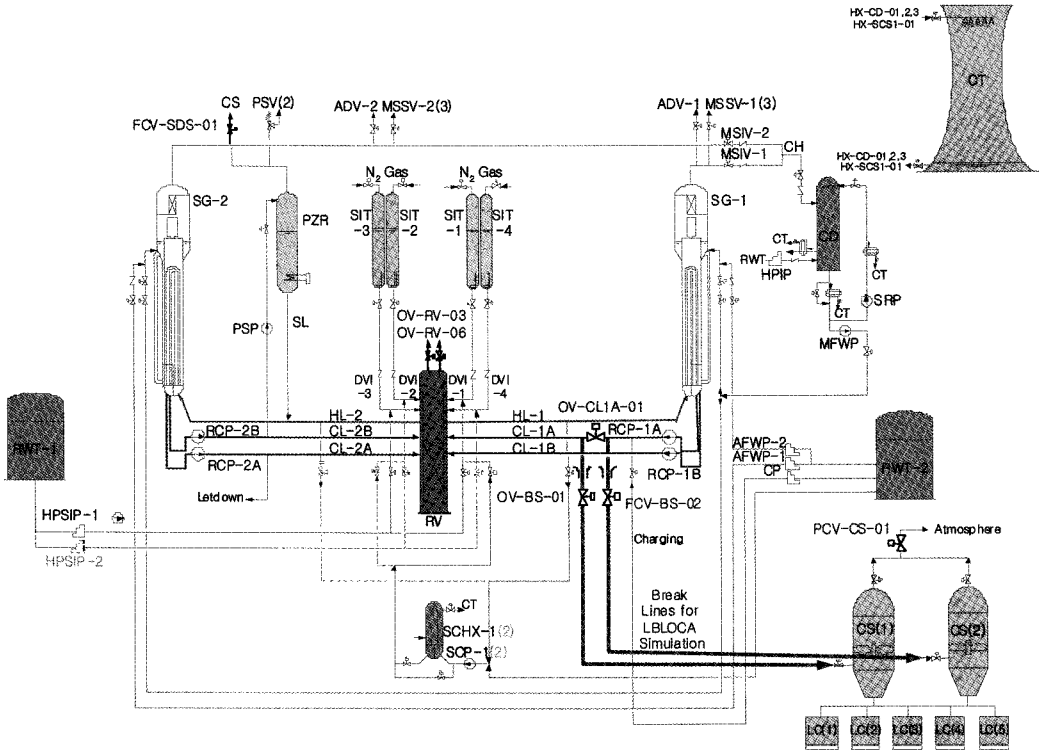

Fig. 1. Schematic Diagram of the Major System of the ATLAS

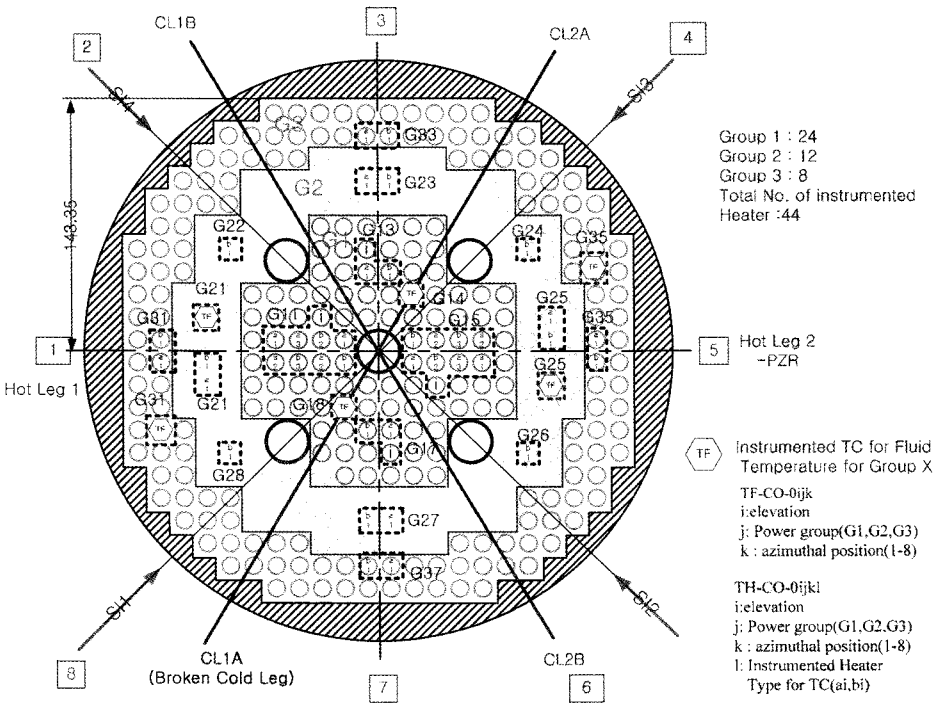

Fig. 2. Schematic View of the Cross-sectional Locations of the Thermocouples for the Cladding (TH) and Fluid (TF) Temperature Measurements

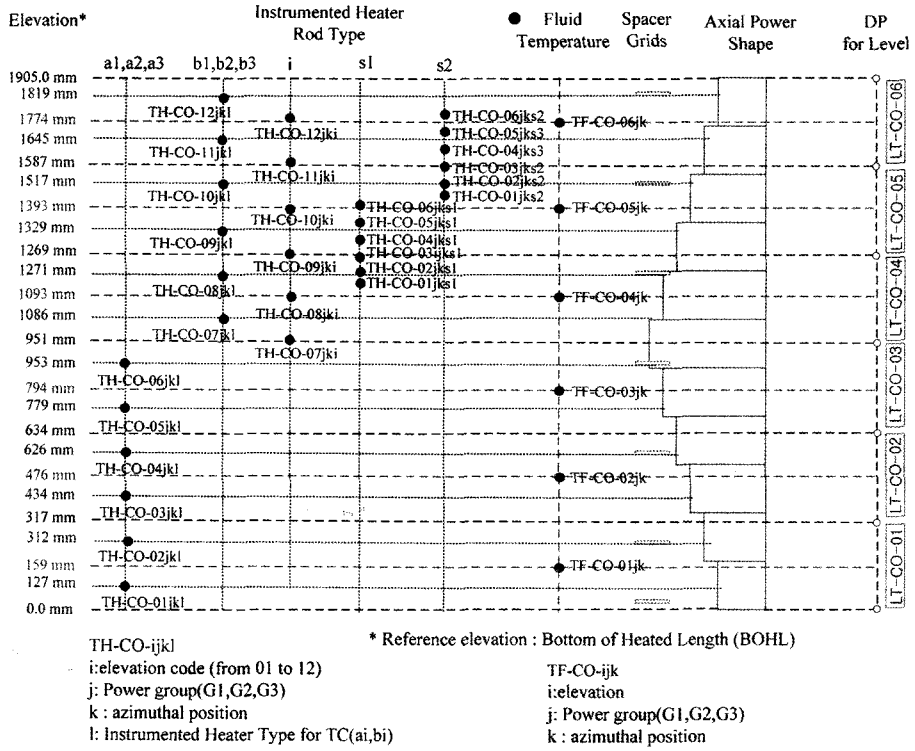

Fig. 3. Axial Power Shape of the Rod Bundle and the Locations of the Thermocouples for the Cladding (TH) and Fluid (TF) Temperature Measurements

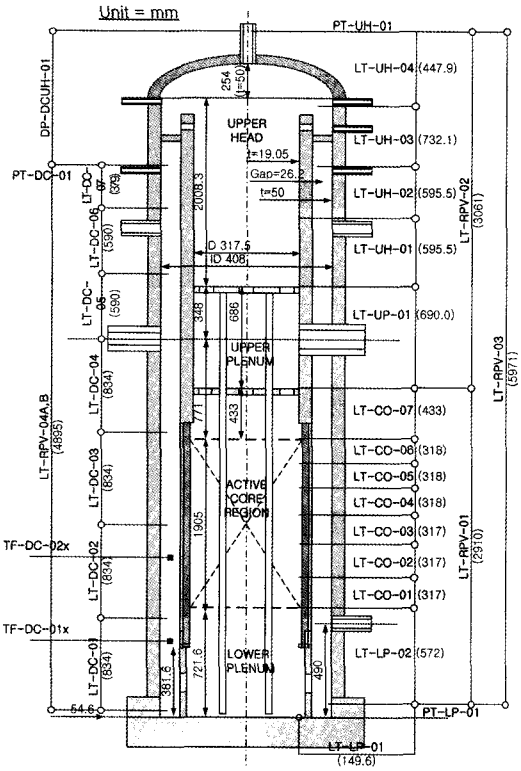

Fig. 4. Vertical Locations of the Transmitters for the Core and Downcomer Water Level

has been built with a hybrid distributed control system (DCS) [8]. Instrumentation signals of the ATLAS consist of measurement-based analog input signals and control-based in-out signals such as AI (Analog Input), AO (Analog Output), TC (Thermocouple), DI (Digital Input), DO (Digital Output), and SR (Serial Communication). The number of instruments is up to 1,236 at present. Instrument signals can also be categorized according to instrument type, such as temperature, static pressure, differential pressure, collapsed water level measured by DP type pressure transmitter, flow rate, power, and rotational speed, etc. More detailed descriptions of the instrument types and data reduction methods for the categorized instrument groups can be found in Cho et al., [8]. The radial and axial distributions of the thermocouples for measuring the core cladding temperatures and the locations of the instruments for measuring the collapsed water levels in the core and the downcomer are shown in Figs. 2, 3 and 4, respectively. To measure the cladding, wall and fluid temperatures in and/or on the core and the downcomer region, more than 430 thermocouples are installed at specified locations; their tagging rules can be indentified in Figs. 2 and 3.

3. TEST CONDITIONS AND PROCEDURE

Since the present experimental tests are not simulated

Table 2. Summary of the Initial and Boundary Conditions for the Present Tests

Variables	Description	LB-CL-09	LB-CL-11	LB-CL-14	LB-CL-15
Power (kW)	after reflood	1065.01 (1.2*ANS-73)	830.9 (1.02*ANS-79)	801.4 (1.02*ANS-79)	466.6 (1.02*ANS-79)
Pressure (MPa)	RPV downcomer	0.12	0.2	0.19	0.13
	SG steam dome	4.8	4.7	4.6	4.5
	CS PCV downstream	0.1	0.15	0.15	0.1
	SIT (initial/reflood)	4.3/2.4	4.3/2.4	4.3/2.6	4.3/2.4
ECC Flowrate (kg/s)	SIT-High Flow	3.58	3.53	3.76	NA
	SIT-Low Flow	1.04	1.13	1.09	NA
	Safety Injection Pump	0.32/0.30 SI-1 & -3	0.30/0.31 SI-1 & -3	0.33/0.32 SI-1 & -2	0.29/0.31/0.30/0.3 SI-1,-2,-3 & -4
Temperture (°C)	RPV wall	204	209	212	190
	SIT/RWT-1	53/53	51/55	55/55	NA/58
	Maximum heater rod surface temperature	465 (Uniform Heating)	459 (Uniform Heating)	546 (Non-uniform Heating)	300 (Uniform Heating)
Level (m, %)	RPV lower plenum	0.53	0.41	0.43	0.5
	SIT / RWT-1	94 / 50	94 / 55	94 / 50	NA / 50
Test Category	-	Conservative condition	Best-estimate condition	Best-estimate condition	Separate effect test

for the whole sequence of the LBLOCA scenario, but only focused on the reflood phase, the initial and boundary conditions, expected in the APR1400 at the start of a reflood phase, should be given to simulate the thermal-hydraulics in the system. The initial and boundary conditions, shown in Table 2, were calculated by applying the scaling ratios of the ATLAS to the MARS calculation results. A single failure of a safety injection system was assumed in the MARS calculation, and thus four SITs and two of the SIPs were working for the LB-CL-09, -11, and -14 tests. For the separated effect test, namely LB-CL-15, however, the injection flow from the SIT was not applied, and only four SIPs were working. For a realistic simulation of the initial experimental condition, some amount of the scaled SIT inventory, which is injected before the start of a reflood phase of the APR1400, was removed from the injected SIT inventory [9]. Four bypass valves between the downcomer and the upper head (two bypass valves), and the hot legs (two bypass valves) were not controlled and they were always fully open during the whole test sequence.

Table 3 shows the sequence of events for the related tests. The actual reflood phase was initiated at 1,912, 1,467, 1,321, and 1,245 seconds after the start of the data acquisition system (DAS) for the LB-CL-09, -11, -14 and LB-CL-15 tests, respectively. As can be observed in Table 3, the 'reflood start' event was preceded by several preparation procedures such as the 'vent' to de-pressurize the primary system and the 'drain' to evacuate the primary water inventory by an opening of the break simulating valves named FCV-BS-01 and OV-BS-01 and the 'power restart' to heat up the cladding temperature and the 'SIT (or SIP) injection'. The water level was located at the lower plenum, which is just below the active core region, at the start of the reflood phase. In these procedures, the water level can be controlled by the drain valves at the RPV bottom and by a fill pump. The core heater power was controlled to follow a specified decay heat, i.e.- 1.2 times that of the ANS-73 decay heat curve for the LB-CL-09 and 1.02 times that of the ANS-79 decay heat curve for the LB-CL-11, -14, and 15 tests as described in Table 2.

4. RESULTS AND DISCUSSION

4.1 General Observations

The collapsed water level of the reactor core (LT-RPV-03) and the downcomer (LT-RPV-04A) is compared with the corresponding quench front locations, estimated from the quench time of the specified thermocouples and their relative elevations, shown in Fig. 5 for the present tests. With an initiation of the SIT injection, for the case of the LB-CL-09, -11, and -14 tests, the water levels of the core

Table 3. Summary of the Major Sequence of Events for the Present Tests

Events	Description	Time			
		LB-CL-09	LB-CL-11	LB-CL-14	LB-CL-15
Data Acquisition Start	Data Recording Start	0	0	0	0
Heating End	Core/RCP Trip, SS Isolation, Heater Power Off	1061	643	533	93
Vent	3 Vent Valves Open (RPV Top, 2 EA, PZR SDS line, 1 EA)	1197	739	623	203
Drain	P<3.0 MPa: FCV-BS-02 20% Open	1534	1076	961	505
	P<2.5MPa: FCV-BS-02 40% Open	1585	1129	1014	563
	P<1.5MPa: FCV-BS-02 100% Open	1623	1169	1056	605
BS Open	P<1.5MPa: OV-BS-01 Open; OV-CL1A-01 Close; Tracing Off; Vent Valves Close	1677	1230	1117	665
IL Drain	Intermediate lines are emptied.	1700	1240	1130	675
Power Restart	After achievement of ICs; 20s linear increase	1855	1399	1244	1175
SIT	Max. T > 450°C (target: 456°C)	1910	1465	1319	NA
Injection	SIT-High Flow (94% ~ 72%)	1930	1492	1344	NA
	SIT-Low Flow (72% ~ 47%)	2033	1621	1451	NA
Test Start (Reflood start)	2.0 s after SIT Injection (for LB-CL-09), 2.0 s after SIP Injection (for LB-CL-15)	**1912**	**1467**	**1321**	**1245**
SIP Injection	12.7 s after Reflood Start (for LB-CL-09), 2.0 s before Reflood Start (for LB-CL-15)	1927	1482	1335	1243
Data Acquisition End	DAS stop	2778.5	2167.5	2230	1805.5

and the downcomer increase rapidly. However, they decrease with a decrease of the ECC flow rate and a spillover of the water inventory. After this level's decreasing period, the water levels increase steadily mainly due to the lowered downcomer wall temperature and the sufficient cooling capacity of the ECC water. For the case of the LB-CL-15 test, however, the collapsed water level of the core and the downcomer increase gradually without a fluctuation due to the low ECC flow rate (about 1.2 kg/s) injected by the SIP. A possible reason for the collapsed water level fluctuation in the core and the downcomer for the case of the LB-CL-09, -11, and -14 tests will be described in section 4.4 of this paper.

Typical cladding temperature behavior of the present experiments measured at the twelve vertical locations of the 'a1' and 'b1' type heater rods as indicated in Fig. 2 can be observed in Fig. 6. As can be seen in Fig. 6, there is a wide temperature scattering at the initiation of the reflood phase at 1,912, 1,467, 1,321, and 1,245 seconds for the case of the LB-CL-09, -11, -14, and -15 tests, respectively, as presented in Table 3. This is mainly due to the applied chopped-cosine axial power shape indicated in Fig. 3 and partly due to the developing thermal boundary layer and an axial conduction to the cold end [10]. As the reflood process progresses, the heater rod experiences a typical quenching process with time; a gradual increase of the cladding temperature to a maximum value, then a gradual decrease followed by a steep decline in the cladding temperature. The maximum temperature measured from the 262 heater cladding thermocouples was up to 722, 558, 615, and 584 °C, and the cladding temperature rise from the start of the reflood to the maximum value, evaluated by using TH-CO-07F11b1, was up to 228, 88, 74, and 255 °C, as indicated in Fig. 6 for the case of the

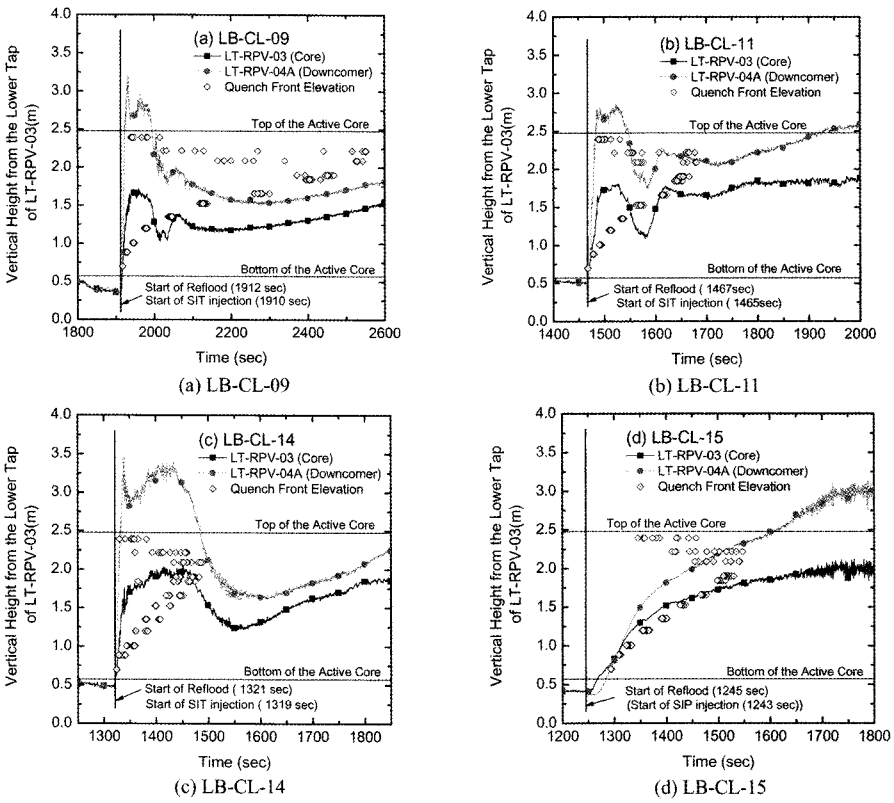

Fig. 5. Collapsed Water Level in the Core and Downcomer Compared with the Quench Front Level

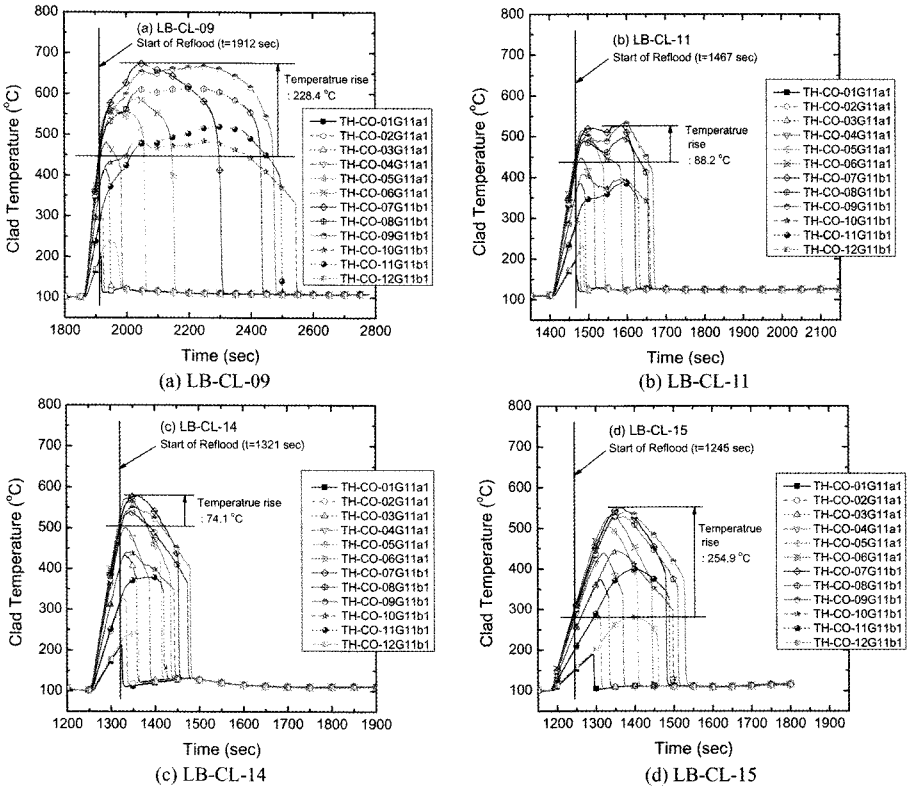

Fig. 6. Cladding Temperature Behavior of the Heater Rod Measured at G11 in Fig. 2 with a Variation of the Vertical Elevations

LB-CL-09, -11, -14, and -15 tests, respectively. As can be observed in Figs. 6(a) and 6(b), during the time span between about 2,000 ~ 2,050 seconds and about 1,550 ~ 1,600 seconds for the LB-CL-09 and -11 tests, respectively, there is a certain degree of temperature excursion at several axial locations. A reason for this temperature excursion will be explained in section 4.4 of this paper.

Generally, in a vertical heated tubular channel, there are several possible flow regimes such as a bubbly, slug, annular and droplet flow regime, etc. [11]. However, Hochreiter et al. [12] indicated that the dominant flow regimes for the post-CHF region in a rod bundle geometry during a reflood phase are an inverted annular regime and a highly droplet dispersed flow regime. Cho et al. [13] maintained that the inverted annular flow regime can be identified by a comparison of the collapsed water level and the corresponding quench front locations, as shown in Fig. 5. Especially, when the flooding velocity is high (up to 0.15 m/sec), the dominant regime above the quench front is an inverted annular regime. In this regime, the rod is covered with a thin layer of vapor and the rest of the channel is filled with subcooled liquid. Therefore, in this regime, the collapsed water level is relatively higher than the quench front elevation [14], as can be seen in Fig. 5. The flooding velocities estimated by a change of the collapsed water level in the lower plenum, LT-LP-02, were about 6.2, 5.2, 6.7, 1.2 cm/sec for the case of the LB-CL-09, -11, -14, and -15 tests, respectively.

The degree of level difference between the collapsed water level and the quench front location is mainly dependant on the length of the inverted annular regime, which depends on the flooding rate, the initial subcooling of the coolant, the system pressure, and the rod bundle initial temperature and the power level. Once the liquid reaches a saturation condition, it breaks into liquid chunks and slugs; dispersed flow may or may not be observed in the far upstream section. The droplets in the dispersed flow are created by sputtering, bubble bursting and entrainment of the liquid from the liquid filaments. With a very low flooding rate condition (less than 0.025 m/s), the liquid reaches a saturation state quickly at or below the quench front and a relatively weak subcooled inverted annular regime can be observed.

Due to the chaotic thermal-hydraulic nature of the reflood phenomena, especially in a rod bundle geometry with an annular downcomer, two-phase flow regimes such as a dispersed droplet flow and a fluctuating bubbly or a slug flow, etc. will be dominant throughout the core region. Therefore, the collapsed water level and the two-phase-mixture level are always different. The former represents the liquid inventory in the channel, while the latter characterizes the heat transfer regimes and also represents the limit of the hydro-dynamically controlled dryout point for the heated surface, which is only wet and in a nucleate boiling below that level. The height of the two-phase-mixture level is generally regarded as a discontinuity in the axial void fraction and in the surface temperature [14].

From the observations shown in Figs. 5 and 6 and from the descriptions above, the qualitative thermal-hydraulic behavior in the core during the reflood phase can be understood. As can be seen in Figs. 5(a) and 5(b) for the LB-CL-09 and -11 tests, respectively, in the lower one-third of the active core, the inverted annular flow regime is dominant. In the middle one-third, the quench front level is always higher than the collapsed water level, which means the two-phase-mixture level is always higher than the collapsed water level. In the upper one-third, top-flooding due to the condensation of steam and the de-entrainment of dispersed droplets governs the quenching phenomena. For the LB-CL-14 test in Fig. 5(c) and Fig. 6(c), due to a larger ECC flow rate and a lower core power level than those of the LB-CL-09 and -11, the whole quench process shows more rapid progress than those of the other two integral effect tests. For the LB-CL-15 test, shown in Fig. 5(d), the effects of the inverted annular flow regime in the lower half are weaker than those of the other tests, mainly due to a relatively low ECC flow rate. Finally, as can be understood by comparing Fig. 5 with Fig. 6, the cladding temperature behavior is closely related to the trend of the collapsed water level in the core.

4.2 Quenching Behavior

The temperature behavior of the heater rod during the reflood phase is characterized by the temperature rise, the turnaround time, the quench time and the quench temperature [15]. The temperature rise is the difference between the cladding temperature at the start of a flooding and the peak temperature reached after a flooding. The turnaround time means the time after a flooding at which the cladding temperature reaches a maximum, $dT/dt = 0$, after which the cladding temperature decreases with time. The quench time indicates the time after a flooding at which the temperature versus time curve starts to drop very rapidly, i.e., almost vertically. This rapid temperature drop results from a sudden rapid increase in the heat removal rate, which is caused by a change in the heat transfer mechanism from dispersed droplet flow film boiling (DFFB) to nucleate boiling [16]. Finally, the quench temperature implies the cladding temperature at which this rapid temperature decrease begins. In the present study, these four parameters were used to compare the behavior of the cladding temperature.

The behavior of the quench temperature and its time along the axial elevation of the active core for the case of the LB-CL-09 and -14 tests can be seen in Fig. 7. A quenching sequence of the cladding progresses from a lower part of the heater rods except for the upper cladding temperatures measured at elevations of 1.517m (TH-CO-10G11b1), 1.645 m (TH-CO-11G11b1), and 1.819 m (TH-CO-12G11b1) above the bottom of the heated length. Moreover, for the case of the LB-CL-09 test, depicted in Fig. 7(a) and Fig. 7(b), a top flooding was more strongly

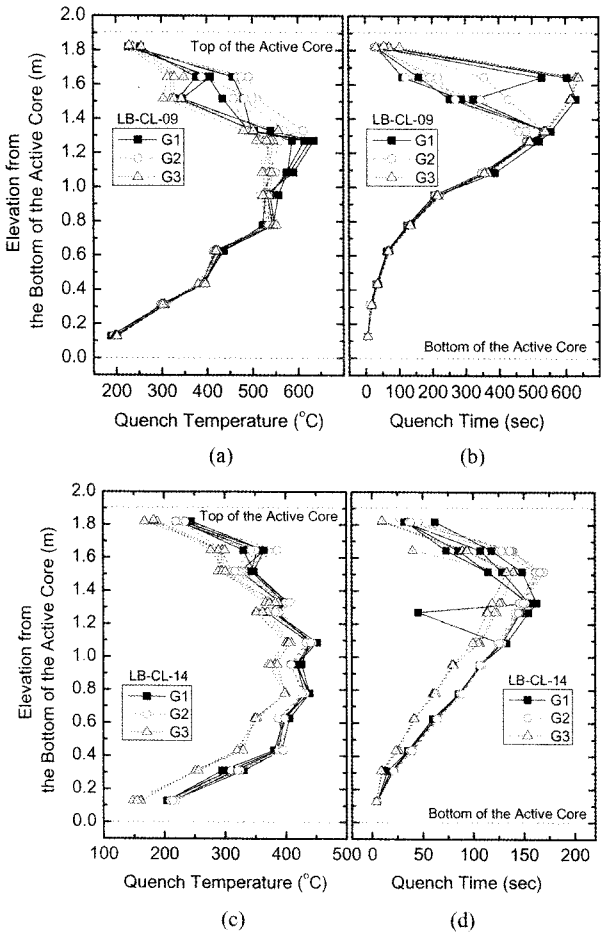

Fig. 7. Behavior of the Quench Temperatures and the Quench Times along the Axial Elevation of the Active Core for the LB-CL-09 and -14 Tests

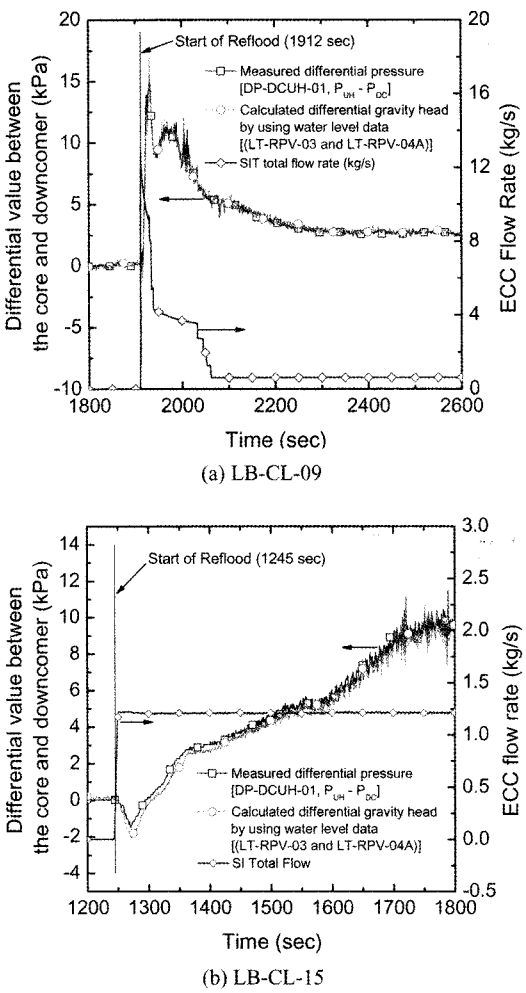

Fig. 8. Pressure Difference between the Core and the Downcomer Compared with the Hydrostatic Head of the Collapsed Water Level for the LB-CL-09 and -15 Tests

observed in heater group-1 (G1 in Fig. 2) and -2 (G2) than in group-3 (G3). Even though further investigation should be carried out, this center oriented top flooding may be a unique phenomenon for the ATLAS. As can be observed in Fig. 7(c) and Fig. 7(d) for the LB-CL-14 test, the cladding temperatures of heater group-3 are lower and the quench times are shorter than those of the other heater groups. This is mainly due to the non-uniform radial power distribution for the LB-CL-14 test. The normalized power factors for heater group-1, 2, and 3 are 1.151, 1.149, and 0.773, respectively.

Top quenching phenomena caused by a falling of the accumulated water (-i.e. top-flooding) at the upper plenum is responsible for this early quenching of the upper-region cladding temperatures. Accumulation of the water at the upper plenum is mainly due to a condensation of the superheated or saturated up-flow steam that contacts the relatively cold upper head structures and a de-entrainment of the droplets, entrained from the near-downstream of the quench front by the decreasing steam velocity that comes from the enlarged flow area. The whole quenching process was finished at 654, 218, 173, and 305 seconds after the initiation of the reflood, and the averaged rewetting velocities estimated by the cladding temperature envelope at each vertical level in the active core region with time are about 0.3, 0.9, 1.1, and 0.6 cm/sec for the case of the LB-CL-09, -11, -14, and -15 tests, respectively.

4.3 Hydrodynamic Interaction between the Core and the Downcomer

For the case of a low flow where the acceleration and viscous forces are negligible, the collapsed water level is equal to the hydrostatic head of the water. A difference in the gravity head can be observed by comparing the water level difference between the core (LT-RPV-03) and the downcomer (LT-RPV-04A), as presented for the LB-CL-09 test in Fig. 8(a) and for the LB-CL-15 test in Fig. 8(b). In the gravity-driven reflooding case, the differential

pressure between the upper plenum and the top of the downcomer is equal to the gravity head difference between the downcomer and the core.

As shown in Fig. 8, the differential gravity head calculated by using the water levels and the measured differential pressures between the upper head and the downcomer show nearly the same trend for these two tests. In particular, the reflooding rate, that is, the actual rate at which the coolant is delivered to the core section during the reflood phase, is the result of a balance between the downcomer hydrostatic head and the core pressure. In summary, the core cooling rate is limited by the height of the downcomer, which determines the maximum head available for reflooding the core. The flooding rate, U_F, is the result of the hydrodynamic balance between the downcomer hydrostatic head and the core head:

$$U_F \propto (h_D - h_C)^{1/2} \quad (1)$$

where h_D is the downcomer head and h_C the core head.

In Fig. 8, the positive differential means that the upper head pressure is higher than that of the downcomer. As can be observed in these figures, the differential pressure behavior is closely related to the ECC injection flow rate. For a large ECC flow, as in the case of the LB-CL-09 test, the downcomer pressure shows a sudden and faster decrease than the core pressure due to the effect of a rapid condensation of the steam in the downcomer caused by the direct contact condensation phenomena with a large amount of the safety injection water. On the other hand, for the case of the LB-CL-15 test, a relatively small ECC flow condition, the downcomer pressure shows a slightly larger increase than the core pressure due to the effect of the evaporation of the ECC injection water and the downcomer boiling caused by heating from the stored energy released from the reactor pressure vessel and the core support barrel. The behavior of the collapsed water level at the initial stage of the reflood for the LB-CL-09 and -15 tests can be observed in Fig. 5(a) and Fig. 5(d), respectively.

4.4 Effect of the Core Water Level with Respect to the Cladding Temperature

In this section, the reason for the collapsed water level fluctuation in the core and the downcomer and the cladding temperature excursions at several axial locations for the LB-CL-09 and -11 tests, mentioned in Figs. 5 and 6, respectively, will be explained. In Fig. 9, the cladding temperature and the water level in the core are compared

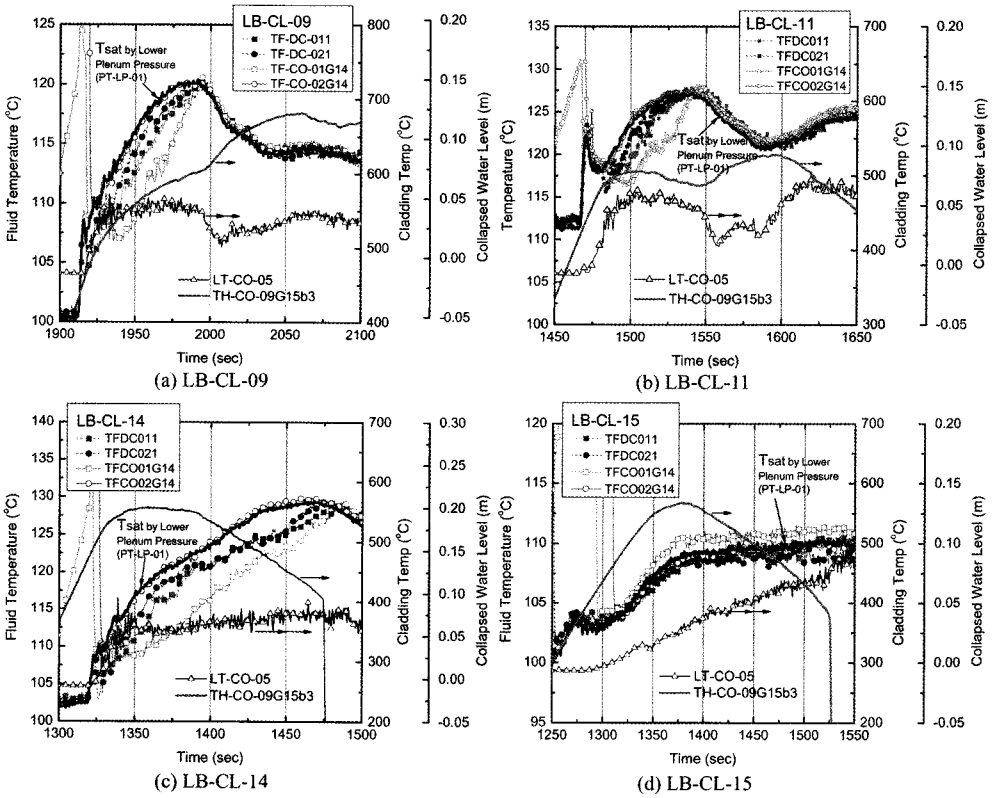

Fig. 9. Comparison of the Fluid Temperature in the Core and the Downcomer with a Variation of the Core Water Level and the Cladding Temperature

with the fluid temperatures in the core and in the downcomer regions for the present tests. The locations of the related instruments can be found in Figs. 2, 3, and 4.

As can be observed in Fig. 5 and Figs. 9(a), 9(b), and 9(c), in the early stage of the reflood, due to the relatively high flow rate of the ECC injection, the water levels in the downcomer and the core increased abruptly and the subcooling degrees of the water inventory in the lower part of the downcomer and the core were also increased as a result. However, with a decreasing ECC flow and the effect of the structural stored energy release, the subcooling degrees of the liquid decreased continuously, and they finally reached a saturation temperature at around 1,993, 1,541, 1,481 seconds for the case of the LB-CL-09, -11, -14 tests, respectively, as can be seen in Figs. 9(a), 9(b), and 9(c). The saturation temperature curve indicated in Fig. 9 was calculated based on the lower plenum pressure, i.e. LT-LP-01. After the injected ECC water in the lower part of the downcomer and the inlet plenum had reached the saturated temperature condition, the core water level, for example measured by LT-CO-05, decreased significantly, as can be observed in Figs. 9(a), 9(b), and 9(c). Therefore, the cladding temperature should be increased. However, after restoring the collapsed water level, the increasing rate of the cladding temperature was reduced, and finally the cladding temperature was decreased again. For the LB-CL-15 test in Fig. 9(d), the fluid temperatures are in a nearly saturated condition from the start of the reflood. However, there is no fluctuation in the water level and the cladding temperature, largely due to the low core power level, as described in Table 2.

From the descriptions above, it can be easily understood that the subcooling degree of the water inventory in the downcomer is an important governing factor for the collapsed water level in the downcomer and the core region. Furthermore, the collapsed water level is closely related to the peak cladding temperature (PCT) during accident conditions. Since the voiding in the downcomer could result in a significant reduction in the downcomer head, this downcomer boiling has become a safety issue by the NRC [17]. The downcomer boiling phenomena resulting from the release of the structural stored energy in the vessel might reduce the flooding rate and cause a significant increase of the peak cladding temperature. In summary, the subcooling degree, which is affected by the downcomer boiling phenomena, has a strong effect on the collapsed water level in the downcomer and the core, and as a result on the cladding temperature behavior.

4.5 Uncertainty Analysis

The uncertainty of measured experimental data is analyzed in accordance with a 95% confidence level. According to the ASME performance test codes 19.1, the uncertainty interval of the present results is given by the root-mean-square of a bias contribution and a precision contribution. The bias and precision errors were evaluated from the data acquisition hardware specifications and the calibration results performed once every year, respectively. Table 4 shows estimated uncertainty levels of each group of instruments [18].

Table 4. Uncertainty Level of Instruments

Items	Unit	Uncertainty
Static Pressure	MPa	0.039
Differential Pressure	kPa	0.23
Collapsed Water Level	m	0.17
Temperature	℃	maximum 2.4
Flow rate	kg/s	0.053

5. CONCLUSION

Three integral effect tests, namely LB-CL-09, -11, 14, and a separate effect test, namely LB-CL-15, for the reflood phase of a LBLOCA were carried out at the ATLAS facility to identify the major thermal hydraulic characteristics in the core region during the reflood phase of a LBLOCA for the APR1400. From an observation of the experimental results, the following conclusions could be drawn:

1) The quenching of the cladding progresses from the lower part of the rods except for the upper part of the active core. Moreover, in the case of the LB-CL-09 test, top flooding was more strongly observed in heater groups-1 (G1) and -2 (G2) than in group-3 (G3).
2) Pressure of the downcomer during the ECC injection is closely related to the ECC flow rate and the structural stored energy, and these two parameters determine whether the steam will be condensed by the ECC water or the injected ECC water will be evaporated by the structural stored energy.
3) The behavior of the collapsed water levels between the downcomer and the core, especially, at the initial stage of the reflood for the integral effect test cases and for the separated effect test case, shows a significantly different trend. For the case of the LB-CL-09 test, the downcomer water level is higher than that of the core region. For the LB-CL-15 test, however, the downcomer water level is lower than that of the core, possibly resulting from the evaporation of the ECC water and from the downcomer boiling effect.
4) For the integral effect test cases such as the LB-CL-09, -11, and -14 tests, the reducing of the subcooling in the lower part of the downcomer and the core region, affected by the downcomer boiling, could result in a significant decrease of the collapsed water level in the core region, and, resultantly, the collapsed water level decrease is responsible for the cladding temperature excursion.

5) For the separated effect test case, namely LB-CL-15, even though the fluid temperatures are in a nearly saturated condition from the start of the reflood, there is no fluctuation in the water level and the cladding temperature due to the low core power level.

ACKNOWLEDGMENTS

This research has been conducted under the nuclear R&D program supported by the Korean Ministry of Education, Science & Technology (MEST).

NOMENCLATURE

d diameter, m
h hydrostatic head, m
l length, m
U velocity, kg/s

Subscript

R the ratio of the ATLAS and the prototype reactor, APR1400
C core
D downcomer

REFERENCES

[1] Yadigaroglu, G., "The reflooding phase of the LOCA in PWRs, Part I: Core heat transfer and fluid flow," *Nucl. Safety*, **19**(1), 20, (1978).
[2] Okubo, T., and Murao, Y., "Assessment of core thermo-hydrodynamic models of REFLA-1D code with CCTF data for reflood phase of PWR-LOCA," *J. Nucl. Sci. Tech.*, **22**, 983, (1985).
[3] Weiss, P., "UPTF experiment: principal full scale test results for enhanced knowledge of large break LOCA scenarios in PWR," NURETH-4, Vol.1, pp.60-66, (1989).
[4] Iguchi, T., Iwamura, T., Akimoto, H., "SCTF-III test plan and recent SCTF-III test results," *Nucl. Eng. Des.*, **108**, 241, (1983).
[5] Baek, W.P., Song, C.H., Yun, B.J., Kwon, T.S., Moon, S.K., Lee, S.J., "KAERI Integral Effect Test Program and the ATLAS Design," *Nuclear Technology*, **152**, 183, (2005).
[6] Ishii, M., and Kataoka, I., "Similarity Analysis and Scaling Criteria for LWRs Under Single Phase and Two-Phase Natural Circulation," NUREG/CR-3267, ANL-83-32, Argonne National Laboratory, (1983).
[7] Park, H.S., et al., "Calculation sheet for the basic design of the ATLAS fluid system," KAERI technical report, KAERI/TR-3333/2007, (2007).
[8] Cho, S., Euh, D.J., Kim, B.D., Choi, K.Y., Park, H.S., Kim, Y.S., Baek, W.P., "Description of the data acquisition-control system and instrumentation of the atlas test facility," WORTH-3 (The 3rd Sino-Korea Workshop in Nuclear Reactor Thermal Hydraulics), Chengdu, China, Aug. (2007).
[9] Park, H.S., et al., "Overview of the KAERI LBLOCA reflood test program using the ATLAS facility," The 7th International Topical Meeting on Nuclear Reactor Thermal Hydraulics, Operation and Safety (NUTHOS-7), Seoul, Korea, Oct. 5-9, paper 350, (2008).
[10] Martini, R., Premoli, A., "Bottom flooding experiments with simple geometries under different ECC conditions," *Energia Nucleare*, **20**(10), 540, (1973).
[11] Wallis, G. B., "One-dimensional two-phase flow," McGrew-Hill Book Company, (1969).
[12] Hochreiter, L. E., Lee, R., Singh, A., Kozuch, J. P., "FLECHT SEASET program final report," Westinghouse Electric Co., WCAP-10926, UNREG/CP-4167, (1985).
[13] Cho, S., Moon, S.K., Choi, K.Y., Park, J.K., Baek, W.P., "Rewetting of a vertical hot surface of a simulated 6x6 rod bundle during a reflood phase," NTHAS5: Fifth Korea-Japan Symposium on Nuclear Thermal Hydraulic and Safety, Jeju, Korea, Nov., (2006).
[14] Sun, K.H., Duffey, R.B., and Peng, C.M., "The prediction of two-phase mixture level and hydro-dynamically controlled dryout under low flow conditions," *Int. J. Multiphase Flow*, **7**(6), 521, (1981).
[15] Cermak, J.O., Kitzes, A.S., Cadek, F.F., Leyse, R.H., Dominicis, D.P., "PWR full length emergency coolant heat transfer (FLECTH) Group I test report," Westinghouse Electric Co., WCAP-7435, (1970).
[16] Cho, S., Moon, S.K., Chun, S.Y., Kim, Y.S., Baek, W.P., 2007. "Spacer grid effects during a reflood in an annulus flow channel," *J. Nucl. Sci. and Tech.*, **44**(7), 967, (2007).
[17] Silva, H.C., Parvez, P., Choe, W. G., "Effect of downcomer boiling on LOCA PCT for a 4-loop PWR with a large-dry containment," The 10th Int. Topical Meeting on Nuclear Reactor Thermal Hydraulics (NURETH-10), Seoul, Korea, Oct. 5-9, (2003).
[18] Kang, K.-H., Moon, S.-K., Park, H.-S., Cho, S., Choi, K.-Y., "ATLAS facility description report," KAERI technical report, KAERI/TR-3754/2009, (2009).